

EMVA 1288 CAMERA CHARACTERISATION AND THE INFLUENCES OF RADIOMETRIC CAMERA CHARACTERISTICS ON GEOMETRIC MEASUREMENTS

Maik Rosenberger¹, Chen Zhang¹, Pavel Votyakov¹, Marc Preißler¹, Gunther Notni¹

¹ Ilmenau University of Technology, Gustav Kirchhoff Platz 2, 98693 Ilmenau, Germany

ABSTRACT

The quality of image sensors and the implementation of them into camera systems is a key fact for image processing applications. Therefore, the EMVA 1288 standard was developed by the European Machine Vision Association. With the measurement information radiometric characteristic of camera systems are described. With this information it is possible to estimate the impact on geometric measurements as well. This paper presents a method which shows the information potential of measured radiometric camera characteristics on the uncertainty of geometric measurements.

Section: RESEARCH PAPER

Keywords: camera characterisation, measurement of camera parameters, measurement system for camera parameters, sensor based edge transition model, optical geometric measurements

Citation:

Section Editor:

Received month day, year; **In final form** month day, year; **Published** month year

Copyright: © year IMEKO. This is an open-access article distributed under the terms of the Creative Commons Attribution 3.0 License, which permits unrestricted use, distribution, and reproduction in any medium, provided the original author and source are credited

Funding: The presented work is the result of the research within the project ID2M which is situated at the Ilmenau University of Technology, Germany as part of the research support program InnoProfile, funded by the Federal Ministry of Education and Research (BMBF) Germany

Corresponding author: Maik Rosenberger, e-mail: maik.rosenberger@tu-ilmenau.de

1. INTRODUCTION

In the last decades of years plenty of different image sensors were developed by a huge variety of companies. Actually there is a strong trend to complementary metal oxide semiconductor (CMOS) based systems. These sensors are easy to integrate in customized camera electronics, due to their high integrated on board digital signal processing as well as their analogue signal processing capabilities. Nevertheless, there are a lot of options which have to be configured by the developer. Nevertheless these circuits have some critical characteristics for example the fixed noise pattern compared to charge coupled device (CCD) based camera systems. As mentioned there is a second great part of image sensors using the CCD technology. One big advantage is the low noise level and the fixed noise pattern in contrast to CMOS systems. On the other side, the developer of camera systems has to take care of the correct routing of the printed circuit board (PCB) and the precise timing for the read out clock generation. In both cases a lot of fine adjustments are necessary to get optimal results out of the image sensor. Those are only a few of the parameters that should be closely observed. That is why one major goal of the characterisation is

to find a way to characterise a camera layout and electronic design during the development process.

The other major goal of the characterisation is application driven. Currently there are a plethora of different camera systems on the market. With this method, system integrators are able to choose an optimal solution for their current imaging problem. For example, if they have to solve a pick and place application the quantum efficiency has a lower priority as the framerate. If they want to have a look to the fundus of the eye or to sample special fluorescence images, the focus should be on high quantum efficiency. Datasheets have some information of main characteristics, but the correct integration on PCB and the correct fine adjustment of parameters are the task of the developer. To compare the implementation of the complete camera system a black box model is assumed, which will be characterized by variation of some significant parameters.

In this paper, a method and a test setup will be described which starts from a signal model considering the imaging chain, calculating important characteristics and close with some test data from a CMOS-based sensor and a CCD-camera system. Moreover, a simulation based method was proposed to evaluate image sensors for geometric measurements using the sensor

parameters in the EMVA 1288 standard. With this simulation method the influences of several sensor parameters were estimated.

2. SIGNAL MODELL AND IMAGE AQUISITION CHAIN

Generally the task of image and radiation sensors is the transformation of electromagnetic radiation into digital or analogue signals. The basic effect for this transformation is called photoelectric effect. For image sensors, which work in the UV-VIS and NIR range, mainly the inner photoelectric effect is used for the transformation of light in to electrical signals.

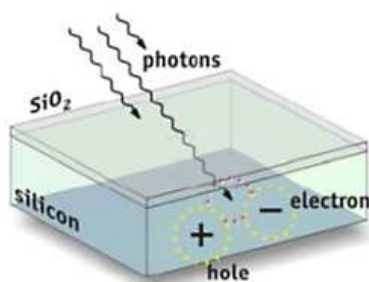


Figure 1: Generation of electron-hole pairs inside the semiconductor [5]

The generated photons from the radiation source hit the sensitive material. Inside the material, a semiconductor, electron-hole pairs (Figure 1) are generated with dependence of the amount of photons. This leads to an accumulation of elementary charge unit e^- inside the material. These charges can be converted into voltages which are depended from the amount of photons which were collected. Inside an image sensor these active area is called pixel, which can be assembled as a CCD or a CMOS element. After this elementary physical effect, plenty of analogue and digital processing has to be done to get a digital value. The following Figure 2 shows the principal way inside a camera system [1]. In consequence to the illustration the assumption for the theory behind the following steps is that the amount of photons is countable. That leads to Poisson models during the model of the transfer processes [2] [3]. According to Figure 2 and in dependence to the exposure time, a special amount of photons hits a pixel and will be partly absorbed. This leads to the generation of a value of charge unit μp . With the weight of the wavelength depended quantum efficiency an average value μe of charge unit can be converted into electrical signals:

$$(1)$$

With this assumption, the effects generated by the fill-factor and the influences of the micro lenses mounted on the active sensor area will be included and not considered separately. The mean number of photons hitting the pixel can be calculated using the knowledge about the pixel area (A), exposure time (t_{exp}) and the irradiance on the sensor surface (E) according equation (2):

$$\mu p = \frac{E \cdot A \cdot t_{exp}}{h \cdot \nu} \quad (2)$$

With the given equations, it is possible to calculate the number of photons μp . For that reason, a precise measurement

of the irradiance measured on the same place where the image

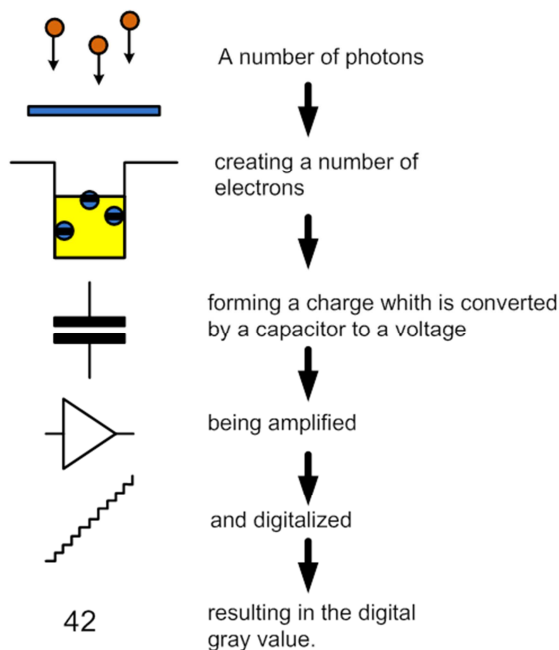


Figure 2: Model of conversion of photons in to digital values [1].

sensor device under test will be proofed is needed.

Therefore a calibrated radiometer should be used. In accordance to the standard, those devices should be recalibrated every year by the manufacturer. The camera electronics converts the radiation which is accumulated into digital values using some stages of amplification and an analog to digital conversion. This behavior can be formulated using the equation (3), according to [1], with the introduction of the overall system gain factor K .

$$(3)$$

In combination with equation (2), the mean gray value μy can be calculated as the sum of the mean value of the dark gray value and the product of overall system gain factor K and expected number of photons μe .

$$\mu y = \mu y_{dark} + K \cdot \mu e \quad (4)$$

With this equation, the linearity of a sensor can be calculated using the gray value of a pixel. As mentioned at the beginning, the accumulation of electron-hole pairs the distribution underlying a Poisson process which can be assumed as equation (5) with the variance and is known as shot noise [1, 3].

$$(5)$$

With the introduction of the quantisation noise σ_q and the signal dependent normal distributed noise σ_d as well as the expected shot noise σ_e , the mean noise measured in the digital signal can be written as equation (6).

$$(6)$$

In combination with the radiation measurement equation (4)-(6), the noise and the overall gain factor K can be determined. Modelling the discussed major influences and system descriptions the graphical illustration is given in Figure 4.

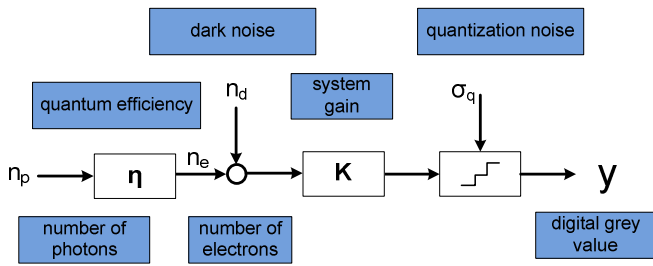


Figure 4: Graphical representation of the system model [1].

For the measurement of these parameters a special measurement setup is demanded in [1] which is developed and displayed in the next chapter. Furthermore, the detailed instruction for the calculation of bad pixels dark current, sensitivity and sensor non-uniformities will be given in the section 2-4 in the standard [1].

3. MEASUREMENT SETUP FOR THE DETERMINATION OF RADIOMETRIC IMAGE SENSOR VALUES

3.1. Test setup construction

The demanded requirements for the measurements to calculate the values discussed in chapter 2 [1] as well as in the complete standard, section 6-9 gives advices for a comparable measurement as well as the restrictions meeting the EMVA criteria. With the knowledge of those requirements, a test setup can be developed. Figure 3 shows the construction of the test

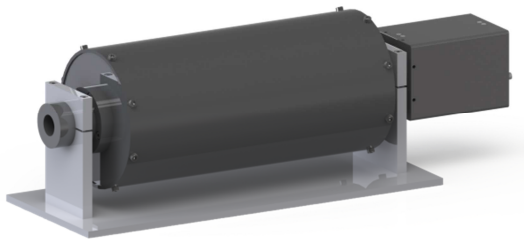


Figure 3: Test setup for measuring the different camera systems.

setup.

The main criteria for the construction was the pinhole camera model which leads to special geometric restrictions:

$$- \quad (7)$$

With the f-number restriction of eight and with the distance d the free radiation diameter D can be calculated. One major point for this construction is the ideal wall surface behavior inside the tube. Therefore, a special painting which has a very low reflection coefficient was used. Furthermore, a special camera socket was constructed for the reason of minimizing the parasitic reflections inside the mounting.

3.2. Test setup software development and structure

The software for the EMVA 1288 measurements was developed using the Matlab framework. The software handles

GigE-Vision cameras as well as pictures taken by the user with other systems. The complete standard was implemented in this measurement tool. For an evaluation of the correctness of the programmed algorithm, the EMVA delivers some simulated data for the verification. This data was used to verify the system.

In the measurements, the irradiance which will be applied to the measurement position of the device under test has to be measured first. With this information; a part of the equations given in chapter 2 can be solved. After the measurement of the radiation power the test camera has to be connected to the

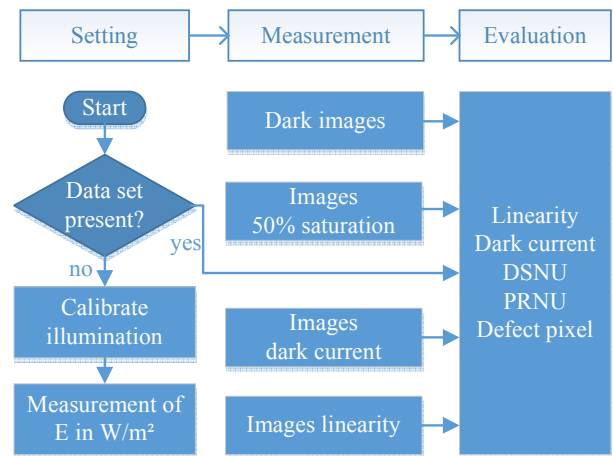


Figure 5: General procedure for data acquisition and evaluation separated in three stages.

setup, afterwards the capturing can be started (Figure 5).

At the end of the camera qualification, a standard compliant EMVA 1288 datasheet of the camera is generated automatically. This datasheet can be used in the simulation program for sensor evaluation. The simulation program was also developed in Matlab. Through an interface the datasheet can be imported into the simulation program. On the basis of the camera system model in Fehler! Verweisquelle konnte nicht gefunden werden. and the measured sensor parameters, a model was developed for the simulation of the 1D edge detection with subpixel accuracy, which is the key process to optical geometric measurements. With this simulation model, the sensor is evaluated according to the simulated measurement uncertainty. This model and its implementation will be described extensively in section 6. In the simulation program, the sensor parameters can be scaled freely in order to estimate the influences of the sensor parameters on the measurement results.

4. MEASUREMENTS OF RADIOMETRIC CHARACTERISTICS

The first measurements were taken with two CCD-camera-systems with different sensors. The sensors have different pixel sizes and different quantum efficiencies. The special characteristic for this measurement is the equal set of the exposure times between the different cameras. So the different saturation levels, as well as the different sensitivity coefficients become visible very clearly in Figure 6.

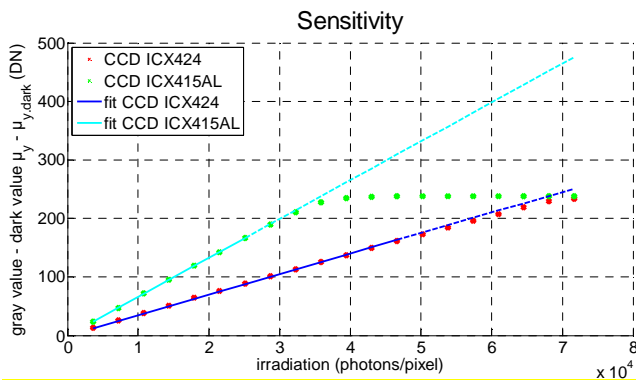


Figure 6: Sensitivity measurements with different camera systems.

Furthermore, the illustration gives a good understanding of what the saturation point is for the camera system. The characteristic saturation point for the CCD 415AL is reached at 34000 photons per pixel.

5. SENSOR EVALUATION FOR GEOMETRIC MEASUREMENTS BASED ON EMVA 1288 SENSOR PARAMETERS

5.1. Combined simulation model

Figure 7 illustrates the process to simulate measurement uncertainty of edge detection with given radiometric sensor parameters. At the first step, a spatial distribution of irradiation in metric units is given as the light signal on the sensor with a stochastic edge location whose subpixel-part is uniformly distributed in $\{0, 1\}$.

Considering the effects of the point spread function of the

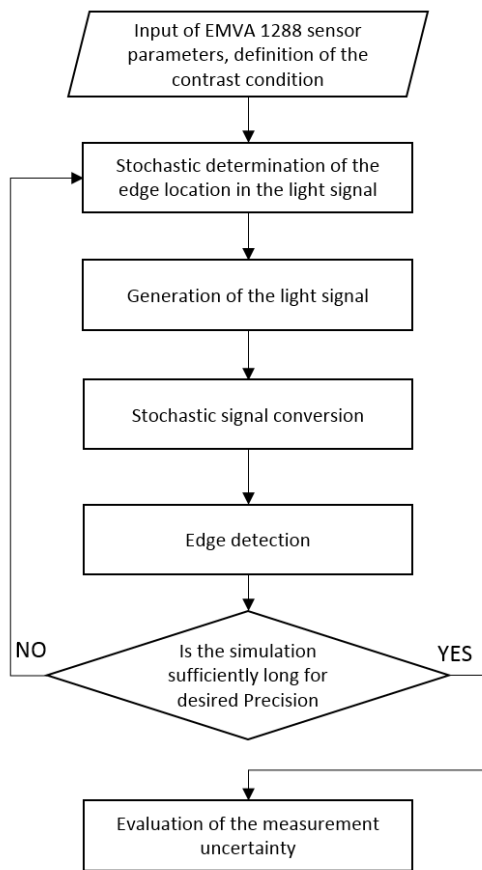


Figure 7: Simulation of measurement uncertainty of edge detection.

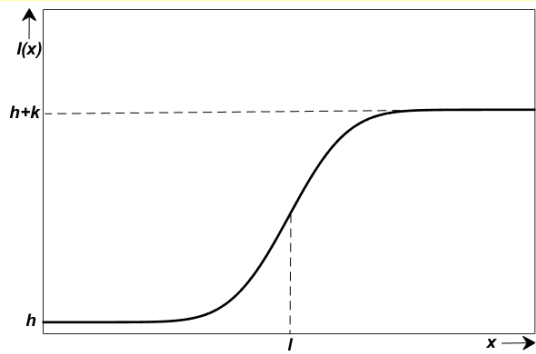


Figure 8: Edge transition using specific blurred edge model.

imaging system, the blurred edge model in [6] (Figure 8) is used, which is represented in equation (8):

$$I(x) = \frac{k}{2} \left(\operatorname{erf} \left(\frac{x-l}{\sqrt{2}\sigma} \right) + 1 \right) + h \quad (8)$$

This signal is converted into a discrete distribution of grey values along a defined number of pixels in the next step. Firstly, the number of photons in each pixel results from integrating equation (8) over the pixel grid L . The number of photons in the n th pixel is calculated by equation (9):

$$\mu_p(n) = \int_{n-L}^{(n-1) \cdot L} 50.34 \cdot t_{exp} \cdot \lambda \cdot I(x) \quad (9)$$

In equation (9) the light wavelength and the exposure time are ignored by setting their value at 550 nm and 1 ms.

From the number of photons, the grey value of each pixel is simulated analogous to the model in Fehler! Verweisquelle konnte nicht gefunden werden.. Upon the assumption that all the pixels have the same linearity error characteristic, the overall quantum efficiency is adjusted for each pixel adapted to the number of in pixel area irradiated photons according to the linearity error curve. The bright signal n_e , namely the number of accumulated electrons is simulated in two steps. Firstly, a number is randomly generated from a Poisson distribution with mean parameter $\eta(\lambda) \cdot \mu_p$. This number is then used as the mean value to generate the number of electrons from a normal distribution, which variance arises from the multiplication of the mean value input and the PRNU1288 value.

Similarly, the dark signal n_d is simulated using a random function of Poisson distribution which mean value is the dark noise value and then a normal distribution which mean value is the outcome of the Poisson function and which variance is the DSNU1288 value.

The bright and dark signals are combined and multiplied with the gain factor K and then quantitated to grey values. The edge location is detected from the grey value signal with an adaptive threshold, which is determined by the histogram based evaluation of all grey values on the signal [7]. To achieve the subpixel accuracy, a polynomial interpolation of third order is implemented to the edge area.

The complete procedure is repeated according to the Monte-Carlo method. The deviation of the detected edge location from the defined location in equation (8) is used as the outcome. Under the assumption that the distribution of the results is subjected to a symmetric distribution function, these outcomes are evaluated with the quantile method for symmetric distributions [7] to calculate the measurement uncertainty.

5.2. Model implementation

In the model implementation the parameters in equation (8) must be determined first. The σ value is to be set according to the characteristic of the optics which will be used in the real measurements. The limit of the high level is determined based on the sensor data using the signal conversion model at one pixel. It is determined in a pre-simulation with this model, with which irradiation value the possibility of pixel saturations equals 95%.

With this value as the upper limit of the light signal, the contrast in equation (8) can be adjusted flexibly for the

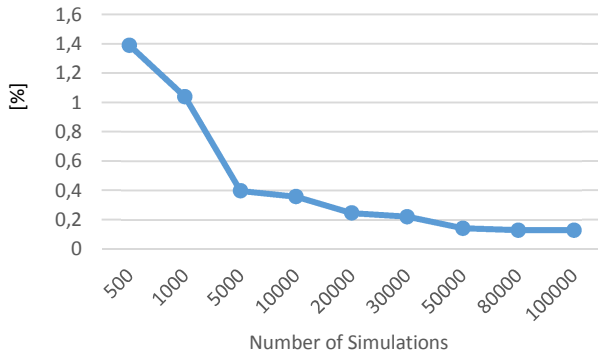


Figure 12: Stability of the Monte-Carlo method in dependency on the number of simulations.

simulation of different measurement conditions.

An important parameter in the Monte-Carlo method is the number of simulations n that must ensure a stable simulation result. Figure 12 illustrates the dependency of the stability on the number of simulations. The ratio of the standard deviation

of the measurement uncertainty to the mean value of measurement uncertainty, which is determined by ten runs, is used as the evaluation criteria. It shows that this ratio remains nearly constant at 0.13 % from $n = 50000$, therefore this value is used for the simulations.

The simulation result with sensor parameters of the CCD-sensor "ICX445" is shown in Figure 10. The deviation of the detected edge location from the target value is distributed approximately symmetrically. Hence the use of the quantile

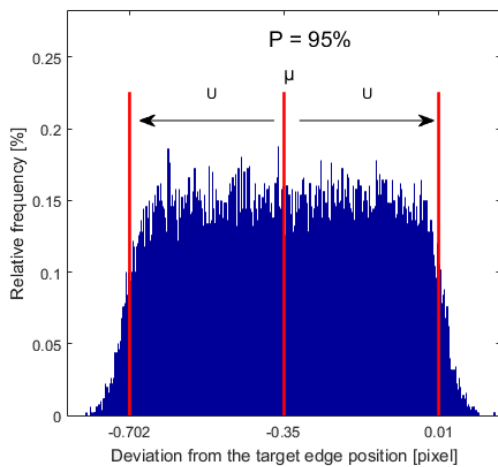


Figure 10: Simulation result with sensor parameters of CCD-sensor "ICX445".

method can be validated.

5.3. Analysis of the influence of sensor data on the uncertainty of measurement

Based on this simulation model and the real characteristics of the CCD-sensor "ICX445", the influences of linearity error, dark noise, DSNU1288 und PRNU1288 of the sensor on the measurements uncertainty was estimated. These four parameters were raised gradually in the tests, while the other system parameters remained unchanged. The σ value in equation (8) is set to 5. The tests were at first performed with 100 % contrast, in which the light signal covers the full dynamic range of the sensor. Then the interaction between the contrast and the influences of sensor parameters was investigated by repeating these simulations under gradually reduced contrast values, which were reached by raising the low level in the light signal. The results of the investigations are represented in Figure 9 to Figure 14. Dark noise and DSNU1288 are given with the absolute unit [e-] in the datasheet, and this unit cannot directly represent their relation to the in 8-bit digitalized signal. Therefore they are represented with the ratio between these parameters and the saturation capacity. Furthermore, a change of systematic measurement deviation is expected with the magnification of linearity error, hence the variations of the expected value of absolute measurement deviation were also observed in this case.

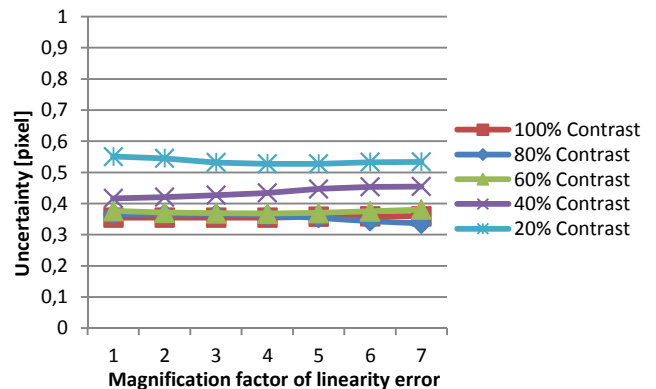


Figure 9: Variation of measurement uncertainty with magnification of linearity error.

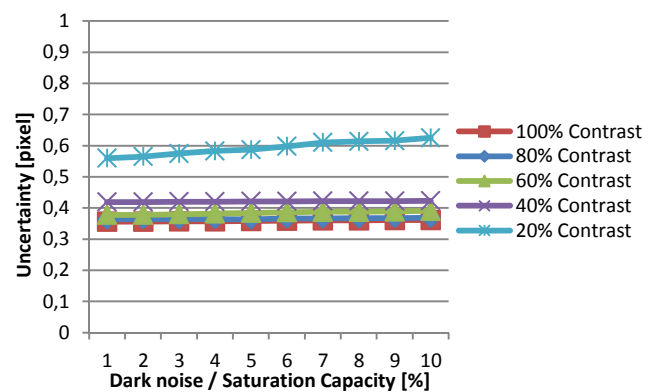


Figure 11: Variation of measurement uncertainty with magnification of dark noise.

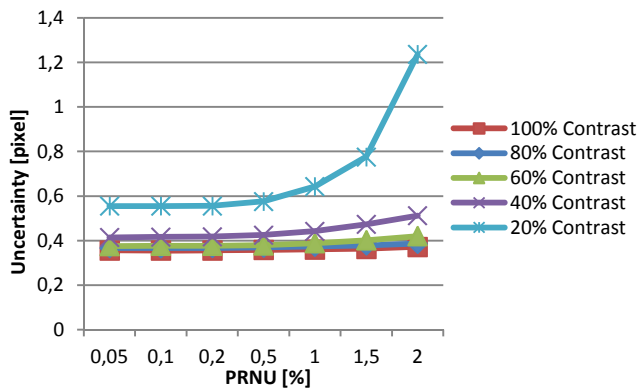


Figure 13: Variation of measurement uncertainty with magnification of PRNU1288.

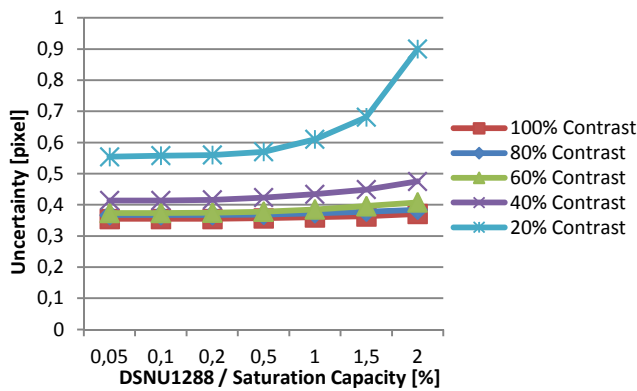


Figure 14: Variation of measurement uncertainty with magnification of DSNU1288.

With 100 % contrast, which could refer to the optimal illumination condition, the magnification of linearity error and dark noise results in hardly any significant change of measurement uncertainty (smaller than 0.005 pixel), as shown in the diagrams, though the magnification of linearity error causes a regular shift of the detected edge location. The magnification of PRNU1288 and DSNU1288 up to 0.5 % of saturation capacity brings about also hardly any changes.

With further magnification a very weak rise of measurement uncertainty can be observed. As these parameters expand to 2 %, the uncertainty rises by approx. 0.015 pixel. As a summary the test results are robust in resistance of a certain deterioration of sensor parameters under optimal contrast conditions, because a wide dynamic range in the converted grey value signal is fundamentally secured in this situation.

As the contrast decreases until to 60 %, the measurement uncertainty curves move slowly upwards with only one exception in Figure 9. With further decrease of contrast this movement becomes significant. The reason for the growth of measurement uncertainty is that the decrease of contrast raises the ratio between the uncertainty of the individual grey values in the signal and its dynamic range by reducing the later value.

On decreased contrast levels the magnification of linearity error can cause an irregular change of uncertainty, whereby the value change is lower than 0.04 pixel. The characteristic of the systematic measurement deviation remains nearly the same in 80 % and 60 % contrast, but changes irregularly heavily in 40 % and 20 % contrast, as shown in figure 15.

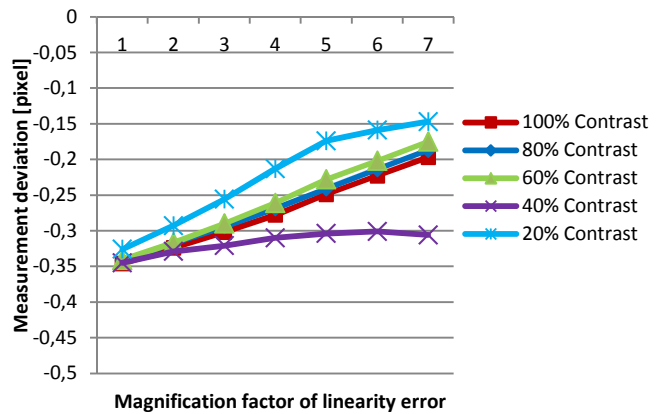


Figure 15: Variation of expected value of absolute measurement deviation with magnification of linearity error.

The reason may be that the linearity error is not regularly distributed over the irradiation levels, as shown in Figure 16, so that the in 40 % and 20 % contrast used sensor dynamic ranges have different overall linearity characteristics.

With the contrast decrease up until to 40 %, the

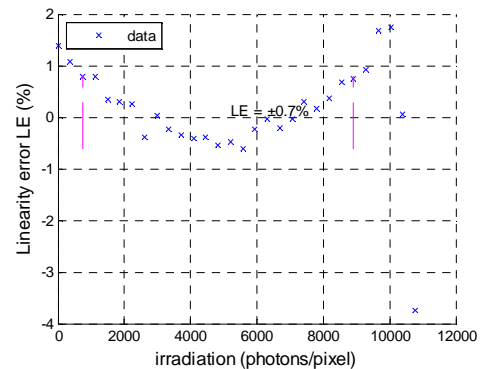


Figure 16: Linearity error curve of CCD-sensor "ICX445".

measurement uncertainty remains stable against the magnification of dark noise. A clear relationship between dark noise and uncertainty can only be observed under the 20 % contrast, whereby the measurement uncertainty rises by 0.063 Pixel, as the dark noise expands to 10 % of the saturation capacity.

A significant interaction between contrast level and sensor parameters can be observed at PRNU1288 and DSNU1288. On the 40 % contrast level, an obvious rise of measurement uncertainty from the turning points at 0.2 % in both curves can be observed, whereby the uncertainty rises by 0.1 pixel with the magnification of PRNU1288 to 2 % and by 0.06 pixel with the magnification of DSNU1288. On the 20 % contrast level the measurement uncertainty increases more significantly. It rises by 0.68 pixel with the magnification of PRNU1288 and by 0.346 pixel with the magnification of DSNU1288.

From the results above, it can be seen that for low light applications and in the case of weak reflective surfaces the sensor parameters PRNU1288 and DSNU1288 have a strong influence on measurement uncertainty in edge detection and should be considered primarily in sensor selection.

6. RESULT DISCUSSION

The magnification of linearity error curve has generally a relatively weak influence on the measurement uncertainty but a significant influence on the systematic measurement deviation. The reason is that the measurement uncertainty results primarily from the uncertainty of the discrete grey values in the edge area, but the linearity error causes only a form distortion of the edge transition signal, which has a direct effect on the systematic measurement deviation. The irregularity of the influence on measurement uncertainty lies in the complex relationship between the signal form and the measurement uncertainty.

A high dark noise reduces the reachable signal-to-noise ratio of the sensor and thus the dynamic range of signal which correlates with the measurement uncertainty. But this effect could become significant only when the contrast in the light signal is reduced to a certain low level or the dark noise is extremely high.

The parameters PRNU1288 and DSNU1288, which refer directly to the uncertainty of the grey values, contribute most to the measurement uncertainty. The reason for the difference of the curve characteristic shown in Figure 13 and Figure 14 is that these parameters represent two different sources of uncertainty. PRNU1288 refers to the uncertainty of the bright signal so that the bright pixels are with higher uncertainties, while the by DSNU1288 characterized dark noise uncertainty is the same to all pixels.

7. CONCLUSIONS

The presented summary shows an abstract of the possibility to characterize image sensors using the standard EMVA 1288 and to evaluate image sensors for geometric measurements using the Monte-Carlo method in which the imaging process is simulated using the system model in the EMVA 1288 standard. With the simulation program, the influences of several essential parameters of image sensor on geometric measurements were investigated.

8. REFERENCES

- [1] European Machine Vision Association, *EMVA Standard 1288 – Standard for Characterization of Image Sensors and Cameras*, www.emva.org, Release 3.0, 2010
- [2] Schmidt, U., *Ein Beitrag zur systemtheoretischen Bewertung von CCD Bildaufnahmesystemen*, PHD Thesis TU-Ilmenau 1993
- [3] Fiete Robert D., *Modeling the Imaging Chain of Digital Cameras*, SPIE Press ISBN 978-0-8194-8339-3
- [4] Jähne, B., *EMVA 1288 Objektive Charakterisierung von Kameras und Bildsensoren*, www.spectronet.de
- [5] Dalsa Coop., *Image Sensor Architectures for Digital Cinematography*, pdf – white paper 03-70-00218-01
- [6] Hagara, M., *Edge Detection with Sub-pixel Accuracy Based on Approximation of Edge with Erf Function*, Radio Engineering; Jun 2011, Vol. 20 Issue 2, p516
- [7] Weißensee, K., *Beitrag zur automatisierbaren Messunsicherheitsentwicklung in der Präzisionskoordinatenmesstechnik mit Bildsensoren*, PHD Thesis TU-Ilmenau 2011